Field Theory Design of Rectangular Waveguide Multiple-Slot Narrow-Wall Couplers

HEINZ SCHMIEDEL AND FRITZ ARNDT, SENIOR MEMBER, IEEE

Abstract —**A compact narrow-wall multiple-slot coupler suitable for inexpensive and very accurate metal-etching manufacturing techniques is proposed and optimized. A computer-aided design theory based on the method of field expansion of eigenmodes considers the effects of finite insert thickness and higher order mode interaction, step discontinuities, and changes in width. Computer-optimized design data for −20-, −8.34-, and −3-dB couplers in the R140-waveguide band (12.4–18 GHz) are given. These data are transferable into other common waveguide bands, e.g., R620 band (50–75 GHz), by suitable frequency scaling calculations. A metal-etched 12-slot coupler prototype for a midband frequency of about 15 GHz achieves a ±1-dB bandwidth of the −3-dB coupling of about 3.2 GHz together with a measured isolation of typically 35–40 dB (minimum 25 dB at the band limits). The measurements show good agreement with theory.**

I. INTRODUCTION

SLOT COUPLING over the whole height of rectangular waveguides on their narrow sides [1] is a well-known technique to build simple but effective directional couplers for a great variety of applications. Although broad-wall coupling generally achieves better broad-band performance than narrow-wall coupling, the latter is especially useful for high-power applications [2]. Common design examples are the short-slot or Riblet hybrid [3]–[6], the Transvar directional coupler [7], and a number of couplers based on the coupled wave theory [8], [9]. These couplers, however, require additional elements for matching or mode suppression purposes [2]–[9], which complicate design and realization.

This paper introduces a narrow-wall multiple-slot coupler, Fig. 1, by which the accurate and inexpensive metal-etching technique may be applied, and which is already advantageously utilized in *E*-plane metal-insert filters [10] and broad-wall couplers [11]. The coupling structure requires no additional matching or mode suppression elements. Optimum coupler performance may be achieved by suitably designing the slot widths and distances along the multislot section.

The computer-aided design is based on field expansion into all incident and scattered waves of interest [10]–[12]. A restriction to TE_{10}, TE_{20}, and TE_{30} modes [2], [13] within the oversized waveguide region is unnecessary. The theory allows direct calculation of the scattering matrix and the immediate inclusion of all significant higher order mode coupling effects between the discontinuities, also below the corresponding cutoff frequencies. Further, finite wall thickness of the coupling section and the discontinuity effect at the abrupt change of the width of the two waveguides are inherently taken into account by this method.

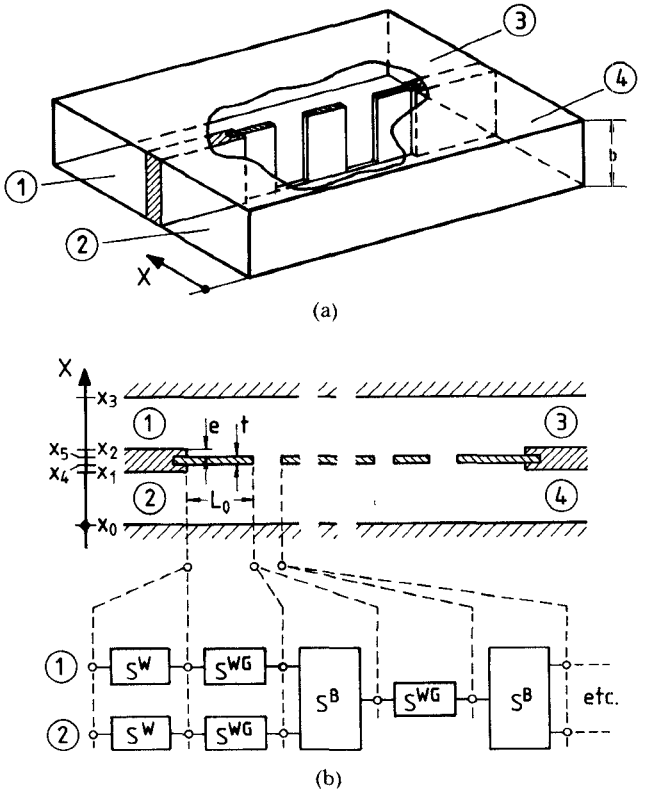

Fig. 1. Multiple-slot narrow-wall metal-insert coupler. (a) Narrow-wall coupled waveguides together with the metal insert containing the coupling slots. (b) Discontinuities with the three building block scattering matrix types: S^W, change in waveguide width; S^B, waveguide bifurcation; S^{WG} (homogeneous) waveguide section.

An optimizing computer program varies the coupler parameters until coupling, transmission loss, and isolation correspond to predicted values. The exclusive use of the scattering matrix in cascading the discontinuities avoids numerical instabilities. Coupling integrals in the ortho-

Manuscript received October 30, 1985; revised February 11, 1986.

H. Schmiedel is with the Deutsche Bundespost, Fernmeldetechnisches Zentralamt, FI 33c, D-6100 Darmstadt, West Germany.

F. Arndt is with the Microwave Department, University of Bremen, Kufsteiner Str., NW 1, D-2800 Bremen 33, West Germany.

IEEE Log Number 8608328.

gonality relations of the field expansion can be evaluated analytically and only a modest number of modes is required to achieve satisfactory convergence.

Data for optimized −20-, −8.34-, and −3-dB couplers in the R140-waveguide band (12.4–18 GHz) are given. The R140-band design data are transferable into the R180 (15–22 GHz), R260 (22–33 GHz), and R620 band (50–75 GHz) by suitable frequency scaling relations. The converted sheet metal thicknesses are commercially available ($t \approx 150$, 100, 50 μm), equal to the related original value for the R140-band design ($t = 190$ μm). Measured results for metal-etched two-slot −20-dB and a 12-slot −3-dB coupler in the R140 band demonstrate agreement with the theory.

II. Theory

Similar to the field theory treatment of broad-wall couplers [11], the coupling section is decomposed into three key building blocks, and the overall four-port scattering matrix of the total coupler (Fig. 1(b)) is calculated by suitable direct combination of all single modal scattering matrices. The derivation of the single modal scattering matrices, however, is quite different from [11], since a TE_{m0}-wave incident at the ports of the discontinuities (Fig. 2), which are uniform along the y direction, excites TE_{n0} modes [14], whereas the E-plane steps of broad-wall couplers [11] require TE^{x}_{mn}-modes [14] to be considered.

The three key building blocks for narrow-wall couplers (Fig. 1) are: the discontinuous change in waveguide width (Fig. 2(a)), with two-port scattering matrix-type S^W (Fig. 1(b)); the waveguide bifurcation with finite wall thickness (Fig. 2(b)), with three-port scattering matrix-type S^B (Fig. 1(b)); and the homogeneous waveguide section, with the known scattering matrix S^{WG}. Therefore, only the field theory derivation of two matrix types S^W and S^B is required.

The fields [14]

$$\vec{E} = \nabla \times \nabla \times \vec{\Pi}_e \quad \vec{H} = j\omega\epsilon \nabla \times \vec{\Pi}_e \tag{1}$$

in each homogeneous subregion (ν) with the general cross-section dimension $c_2^\nu - c_1^\nu$ and a narrow-wall side at $x = c_3^\nu$ (cf. Fig. 2(a)) are derived from the y-component of the electric Hertzian vector potential $\vec{\pi}_e$, which is assumed to be a sum of suitable eigenmodes satisfying the vector Helmholtz equation and the boundary conditions [15]

$$\Pi_{ey} = \sqrt{\frac{2}{(c_2^\nu - c_1^\nu)b}} \sum_{i=1}^{I} \frac{1}{\sqrt{Z^\nu_{FHi}}} \cdot \frac{1}{\beta_i^\nu \omega\epsilon} \sin\left[k_c^\nu (x - c_3^\nu)\right] \cdot \left[A_i^\nu e^{-j\beta_i^\nu z} + B_i^\nu e^{+j\beta_i^\nu z}\right] \tag{2}$$

with

$$Z^\nu_{FHi} = \frac{\omega\mu}{\beta_i^\nu}$$

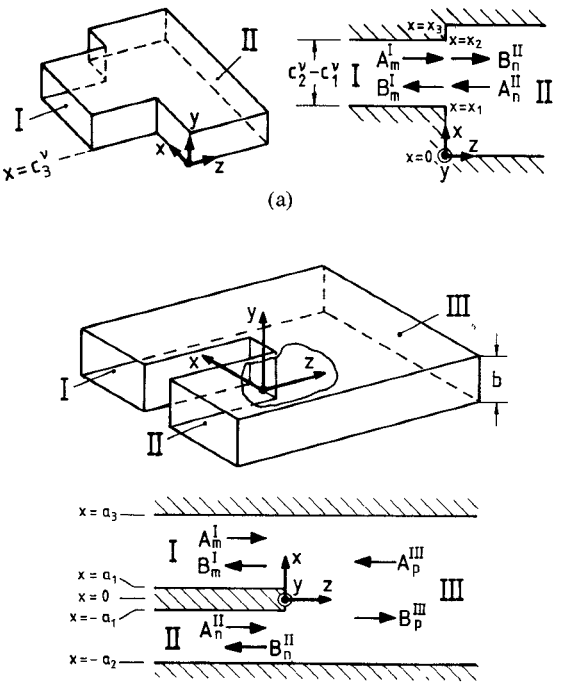

(a)

(b)

Fig. 2. Key building blocks to describe the coupling section exactly by field theory methods. (a) Change in waveguide width, scattering matrix S^W. (b) Waveguide bifurcation with finite wall thickness taken into account, scattering matrix S^B.

and

$$\beta_i^\nu = \begin{cases} \sqrt{\omega^2\mu\epsilon - k_c^{\nu 2}} & \omega^2\mu\epsilon \geq k_c^{\nu 2} \\ -j\sqrt{k_c^{\nu 2} - \omega^2\mu\epsilon} & \omega^2\mu\epsilon < k_c^{\nu 2} \end{cases}$$

$$k_c^\nu = \frac{i\pi}{c_2^\nu - c_1^\nu}.$$

As in [10]–[12], [14], [15], the eigenmodes (2) are suitably normalized so that the power carried by a given wave is 1 W for a wave amplitude coefficient of $1/\sqrt{W}$.

The still unknown amplitude coefficients A_i^ν, B_i^ν in (2) are related to each other by matching the tangential field components along the corresponding interface at the step discontinuity under consideration [10]–[12], [14], [15]. This directly yields the related modal scattering matrix. For computer optimization, the expansion into 15 eigenmodes at each discontinuity has turned out to be sufficient. The final design data are checked up to 30 eigenmodes. As has already been stated [16], [17], there is no need to maintain this number of "localized" [16] modes, necessary for calculating the scattering matrix of the H-plane discontinuity, for the "accessible" [16] modes with a homogeneous waveguide section between them. The modal scattering matrix method utilized, however, allows one to take advantage of this fact.

A. Change in Waveguide Width (Fig. 2(a))

With regard to the desired description of the overall coupler by means of the scattering matrix (cf. Fig. 1(b)), instead of introducing a wide-band network [16], the direct

derivation of the modal scattering matrix of the H-plane step discontinuity is preferred. The eigenmodes in the subregions I and II (Fig. 2(a)) are given by (2) for $(c_2^{\mathrm{I}} - c_1^{\mathrm{I}}) = (x_2 - x_1)$, $c_3^{\mathrm{I}} = x_1$, $i = m$, and $(c_2^{\mathrm{II}} - c_1^{\mathrm{II}}) = x_3$, $c_3^{\mathrm{II}} = 0$, $i = n$, respectively. Matching the fields at $z = 0$ leads to the relation

$$\begin{pmatrix} B^{\mathrm{I}} \\ B^{\mathrm{II}} \end{pmatrix} = (S^W) \begin{pmatrix} A^{\mathrm{I}} \\ A^{\mathrm{II}} \end{pmatrix} \tag{3}$$

with the two-port scattering matrix of the change in width

$$(S^W) = \begin{pmatrix} (q)^{-1}(r) & 2(q)^{-1}(Y_n)(1/\beta_n) \\ 2(s)^{-1}(Y_m) & (s)^{-1}(t) \end{pmatrix} \tag{4}$$

where the abbreviations are elucidated in the Appendix.

B. Waveguide Bifurcation with Finite Wall Thickness (Fig. 2(b))

The modal scattering matrix of this discontinuity has already been derived in [10]. For completeness, however, the results are reproduced at this place using the present notation.

The eigenmodes in the subregions I, II, III (Fig. 2(b)) are given by (2) for $(c_2^{\mathrm{I}} - c_1^{\mathrm{I}}) = (a_3 - a_1)$, $c_3^{\mathrm{I}} = a_1$, $i = m$, $(c_2^{\mathrm{II}} - c_1^{\mathrm{II}}) = (a_1 - a_2)$, $c_3^{\mathrm{II}} = -a_2$, $i = n$, and $(c_2^{\mathrm{III}} - c_1^{\mathrm{III}}) = (a_3 + a_2)$, $c_3^{\mathrm{III}} = -a_2$, $i = p$, respectively. Matching the fields at $z = 0$ leads to the relation

$$\begin{pmatrix} B^{\mathrm{I}} \\ B^{\mathrm{II}} \\ B^{\mathrm{III}} \end{pmatrix} = (S^B) \begin{pmatrix} A^{\mathrm{I}} \\ A^{\mathrm{II}} \\ A^{\mathrm{III}} \end{pmatrix} \tag{5}$$

with the three-port scattering matrix of the waveguide bifurcation

$$(S^B) = \begin{pmatrix} -h(I_{2pm})(Z_m) & -g(I_{1pn})(Z_n) & +(Z_p) \\ (Y_m) & (0) & h(I_{2pm})^T(Y_p) \\ (0) & (Y_n) & g(I_{1pn})^T(Y_p) \end{pmatrix}^{-1} \cdot \begin{pmatrix} h(I_{2pm})(Z_m) & g(I_{1pn})(Z_n) & -(Z_p) \\ (Y_m) & (0) & h(I_{2pm})^T(Y_p) \\ (0) & (Y_n) & g(I_{1pn})^T(Y_p) \end{pmatrix} \tag{6}$$

where the abbreviations are elucidated in the Appendix.

In order to preserve numerical accuracy, the direct combination of the involved scattering matrices at all step discontinuities (cf. Fig. 1) is used [12], as opposed to the common treatment by transmission matrices. Since the direct combination of scattering matrix parameters contains exponential functions with only negative argument, this procedure, although somewhat more extensive, avoids numerical instabilities caused by the otherwise known situation of interacting discontinuities if evanescent modes are involved. A further advantage of this direct combination is that no symmetry of ports (i.e., "modes") is required. Since the "accessible" [16] modes include only the propagating modes and the first few evanescent modes, depending upon the distance between adjacent discontinuities [16], [17], the utilization of this unsymmetry helps to reduce computing time and storage requirements. For example, for the "long" coupler versions (cf. Table I) where the slots are separated by lengths L_1, L_2, which are not the optimum short solution, only five "accessible" modes are sufficient.

The equations for cascading two two-ports by the related scattering matrices are given in [12]. The direct combination of a two-port with a three-port scattering matrix, also necessary to calculate the total coupling section (cf. Fig. 1) for completeness, is treated in the Appendix.

TABLE I
COMPUTER OPTIMIZED DESIGN DATA FOR NARROW-WALL METAL INSERT COUPLERS IN THE R140 BAND (WR62 HOUSING: 15.799 MM × 7.899 MM)

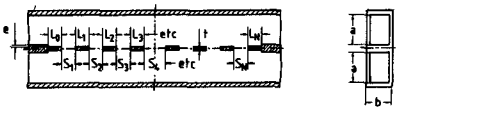

Coupling in (dB)	Number of Slots N	Metal Insert Thickness t (mm)	Slot Lengths (mm) S_1	$S_2 \cdots S_{N-1}$	S_N	Intermediate Lengths of Waveguide Section (mm) L_0	$L_1 \cdots L_{N-1}$	$L_2 \cdots L_{N-2}$	$L_3 \cdots L_N$	Width a (mm)	Midband Frequency (GHz)	± 1dB Bandwidth of the Coupling (GHz)	E Minimum Isolation (dB)	Remarks
-8.34 [1]	6	0.19	1.896	5.508	6.556	40 [2]	1.817	1.501	1.027	10 [2][4]	14.5	1	28	
-20	6	0.19	1.52	2.01	3.87	50	2.24	2.19	2.43	0	15.5	2.5	50	
-8.34	6	0.19	0.33	0.28	8.46	50	12.69	11.45	0.26	0	13.5	2.1	26	long [3]
-3.01 [3]	12 [3]	0.19	1.90	5.61	6.56	23.7	1.82	1.50	1.03	0	16	5.3	26	
-3.01 [3]	12 [3]	0.19	2.26	5.44	6.33	23.7	1.72	1.31	1.34	0	14.5	3.6	30	
-3.01 [3]	12 [3]	0.19	0.10	0.01	8.03	23.7	12.7	11.28	0.44	0	13.6	3.8	26	long [3]
-3.01 [3]	12 [3]	0.19	3.18	5.44	6.84	23.7	1.08	1.16	0.95	0.5 [4]	16	4.2	22	
-3.01 [3]	12 [3]	0.19	2.51	4.86	6.48	23.9	0.78	0.58	0.53	0.25 [4]	15.1	4.4	30	cf. Fig. 6 a
-3.01 [3]	12 [3]	0.19	3.0	5.2	6.6	23.9	1.30	1.40	1.20	0.25 [4]	15.1	3.2	25	cf. Fig. 6 b

1) Partial results see Figs 3c, 4
2) in Fig 4 variable
3) Tandem connection of two symmetrical -8.34 dB coupling sections (separated by L_0) with six slots each, but complete -3 dB structure optimized
4) included in the optimization process
5) i.e. intermediate lengths of waveguide sections L_1/L_2 are not the optimum short solution (less sensitive to higher order mode interaction)

III. DESIGN

As with metal insert filters [10] and broad-wall couplers [11], the computer-aided design is carried out by an optimizing program applying the evolution strategy method [15], [18]. An error function $F(\bar{x})$ to be minimized is defined

$$F(\bar{x}) = \sum_{v=1}^{V} \left(\frac{|S_{21}(f_v)|}{S_{21D}} \right)^2 + \left(\frac{|S_{41(f_v)}| - S_{41D}}{S_{41T}} \right)^4 \overset{!}{=} \mathrm{Min} \tag{7}$$

where V is the number of frequency sample points f_v, S_{21D}, S_{41D} are the desired given isolation and coupling coefficients in decibels, S_{21}, S_{41} are the calculated scattering coefficients of the coupler at the frequency f_v, and S_{41T} is the given tolerated deviation (not equal to zero) of the coupling in decibels. Also, for the given waveguide housing dimensions, thickness t of the coupling metal insert, and

number of coupling slots, the parameters $\bar{x}$ to be optimized (Table I) are the slot and the intermediate coupling wall lengths.

IV. Results

Fig. 3 illustrates the convergence behavior of the field expansion method in relation to the number I of the modes considered in (2). For the two discontinuity types, change in waveguide width (Fig. 3(a)) and the bifurcation (Fig. 3(b)), the real part of the electrical-field strength E_y is plotted versus the normalized cross distance. For these investigations, the $z = 0$ cross sections in Fig. 3(a) and (b) are considered, where in Fig. 3(a) the tangential component E_y has to be zero for $x > 2b$ (conducting plane). A fundamental model incidence at port ① of Fig. 3(b) is assumed and all ports are considered to be ideally matched. At $z = 0$, therefore, in Fig. 3(b), the only significant field amplitudes are that one incident in region ①, and that one transported within the corresponding $2.05b < x < 4.1b$ portion of region ③. It may be stated that for $I = 15$, or $I = 10$ modes, respectively, the discontinuity may be considered to be sufficiently approximated. Fig. 3(c) shows the convergence behavior of the magnitude of the scattering coefficients S_{21} (isolation) and S_{41} (coupling) of a −8.34-dB six-slot coupler as a typical design example (cf. Table I). Also, for about 15 modes, sufficient asymptotic behavior for optimization purposes may be stated. Similar results are obtained by other examples. Fig. 3(c) further indicates that the order of modes necessary for suitable convergence does not vary considerably with frequency (cf. the parameter b/λ_0) since the technique of directly combining the scattering matrices avoids numerical instabilities.

The influences of the step width e at the discontinuity change in waveguide width (between the common narrow wall of the waveguides and the coupling metal insert containing the metal-etched slots, cf. Fig. 1(b)), as well as of the length L_0 between this step and the first slot, are demonstrated in Fig. 4, at the example of a −8.54-dB six-slot coupler (cf. Table I). As expected, increasing e leads to decreasing coupling. For practical designs, therefore, the step width e should either be reduced to a negligible value (e.g., by means of a smooth transition) or has to be taken into account for the optimization process. Fig. 4(b) indicates that the intermediate waveguide section between the step discontinuity and the first slot should be of sufficient length L_0 (e.g., in the R140 band $L_0 >$ 40 mm), to reduce the discontinuity effect, or has to be taken into account in the calculations.

Fig. 5 shows the calculated and measured magnitude of the scattering coefficients S_{41} (coupling) and S_{21} (isolation) of a two-slot R140-band waveguide −20-dB coupler. The thickness of the metal insert is $t = 100$ μm. The computer optimized design data are normalized to the waveguide height $b = 7.899$ mm. The measured results are found to be in good agreement with the theory.

Computer-optimized design data for R140-waveguide narrow-wall couplers are presented in Table I. Six-slot

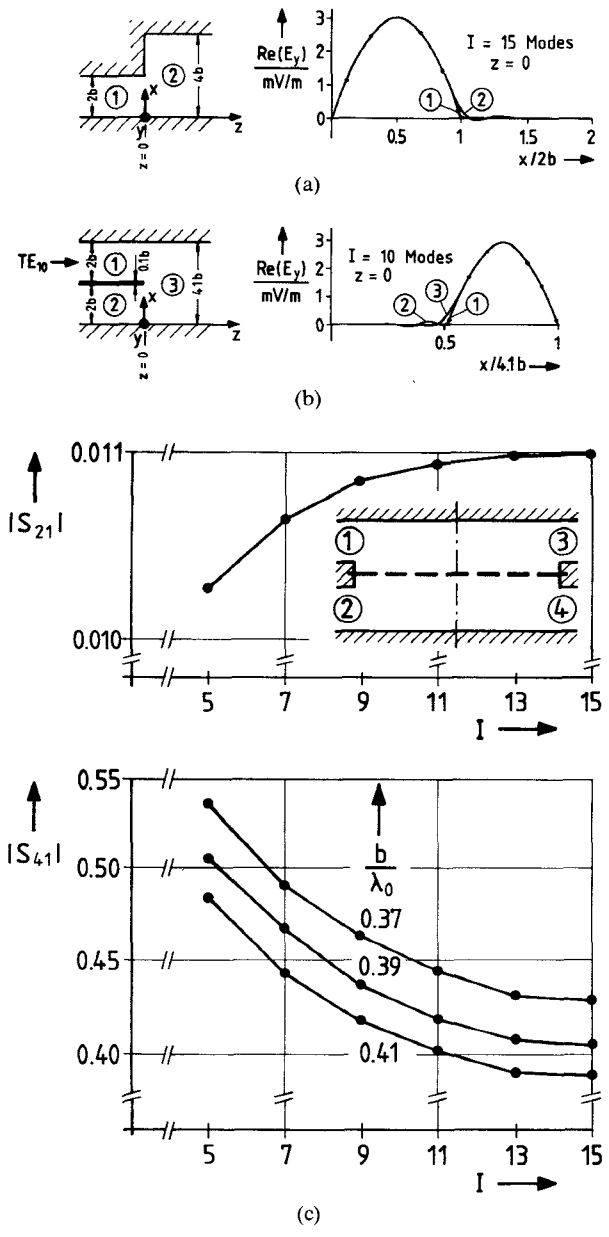

Fig. 3. Illustration of the convergence behavior of the field expansion method. (a) Discontinuity change in waveguide width. Real part of the electrical field strength E_y plotted versus normalized cross-distance $x/(2b)$ at $z = 0$; number of modes considered, cf. (2), $I = 15$; the circled numbers correspond to the related subregion. $b/\lambda_0 = 0.3$. (b) Discontinuity waveguide bifurcation. Real part of the electrical field strength E_y plotted versus normalized cross-distance $x/(4.1\ b)$ at $z = 0$; number of modes considered $I = 10$; TE_{10}-wave incidence in port 1. $b/\lambda_0 = 0.35$. (c) −8.34-dB six-slot coupler. Magnitude of the scattering coefficients S_{21} (isolation) and S_{41} (coupling) as a function of the number I (cf. (2)) of modes considered at each discontinuity. b = waveguide height, λ_0 = free-space wavelength. The coupler dimensions are given in Table I.

−20- and −8.34-dB couplers, as well as 12-slot −3.01-dB couplers (tandem connection of two −8.34-dB coupling sections), are chosen for design examples. The minimum isolation of the −3.01-dB couplers is chosen to be 20–30 dB for bandwidths of about 30 percent; higher isolation, e.g., 40 dB if required, is given within smaller bandwidths (cf., e.g., Fig. 6(a)). Due to the different coupling mechanism [2], however, narrow-wall multi-element couplers do

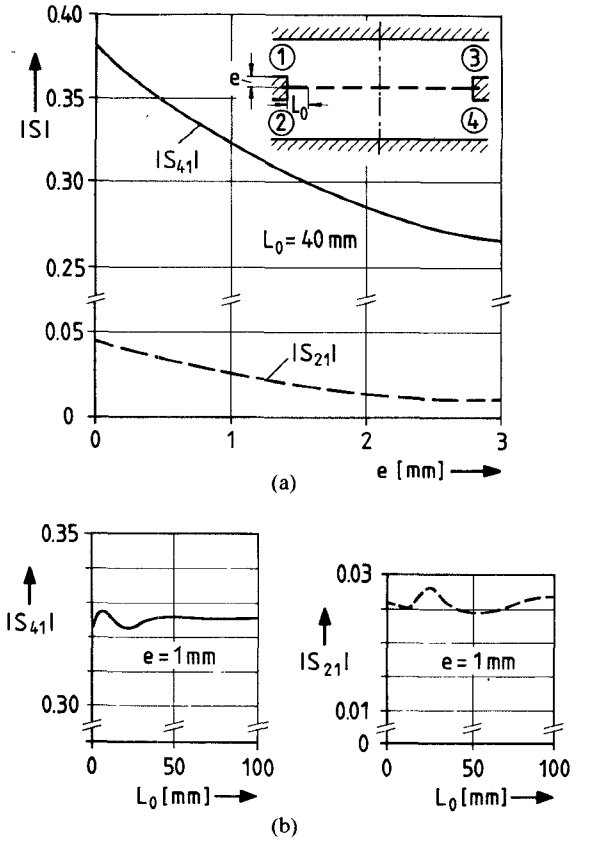

Fig. 4. Illustration of the influences of the step width e (at the discontinuity change in waveguide width) as well as of the length L_0 between this step and the first slot. $b/\lambda_0 = 0.41$. -8.34-dB six-slot coupler (cf. Table I). (a) Influence of the step width e. (b) Influence of the length L_0 on the scattering parameters $|S_{41}|$ (coupling) and $|S_{21}|$ (isolation).

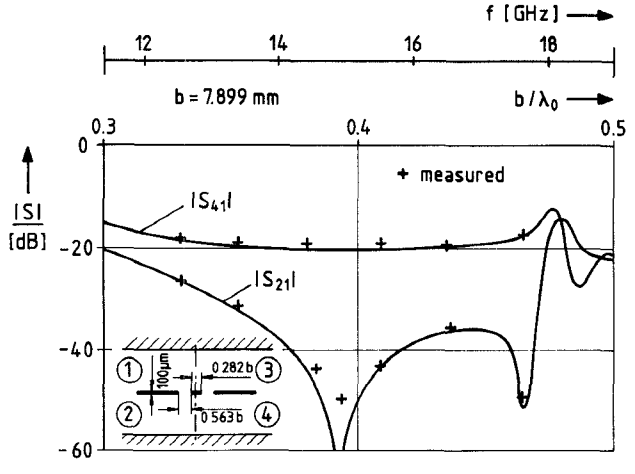

Fig. 5. Two-slot -20-dB coupler. Calculated and measured magnitude of the scattering coefficients S_{21} (isolation) and S_{41} (coupling) as a function of the waveguide height b normalized to the free-space wavelength λ_0, as well as of the frequency f. R140-band waveguide: $a = 15.799$ mm, $b = 7.889$ mm, + measured (measuring limit -50 dB).

not achieve the broad-band performance that may be attained by their broad-wall counterparts [11].

The data in Table I may be transformed by suitable frequency scaling calculations into other common frequency bands. As has been proved by exact analysis, the transformation of all geometrical dimensions (including

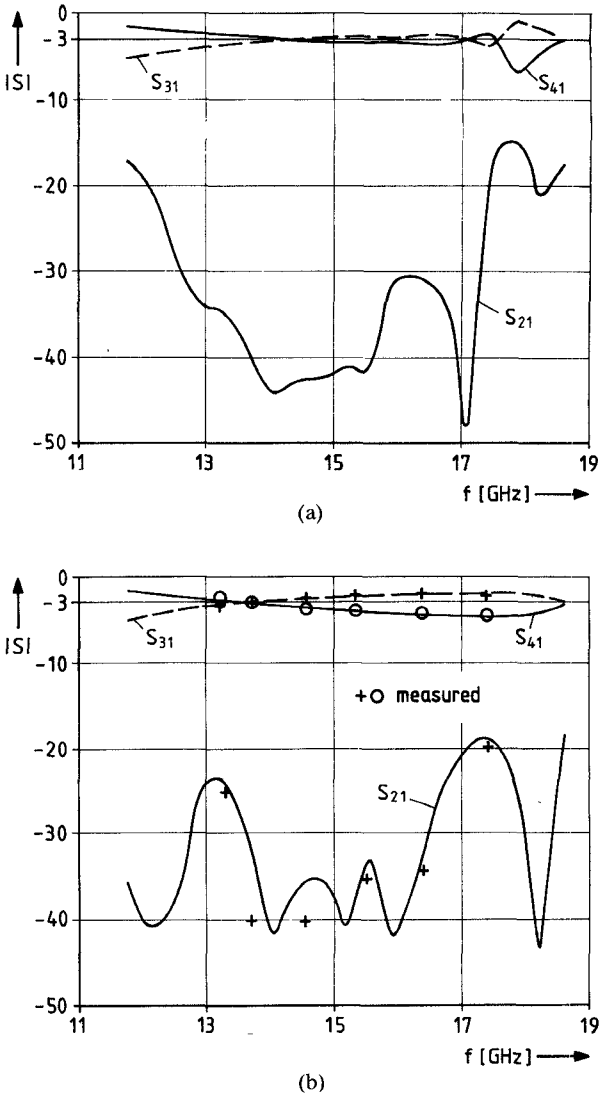

Fig. 6. Twelve-slot -3-dB coupler (tandem operation of two -8.34-dB sections). Magnitude of the scattering coefficients S_{21} (isolation), S_{41} (coupling), and S_{31} (transmission) as a function of the frequency f. R140-band waveguide: $a = 15.799$ mm, $b = 7.899$ mm. (a) Optimum design (Computer optimized data: cf. Table I). (b) Realized design (Data: cf. Table I). + measured.

the coupling sheet-metal thickness t) with the related cutoff frequency ration $\lambda_{cnew}/\lambda_{cR140}$ yields only slight deviation of the coupler behavior compared with optimized results. The coupling sheet-metal thickness scaled up to the R180 band ($t \approx 150$ μm), R260 band ($t \approx 100$ μm), and R620 band ($t \approx 50$ μm) are also commercially available.

Fig. 6 shows the magnitude of the scattering coefficients S_{21} (isolation), S_{41} (coupling), and S_{31} (transmission) as a function of the frequency for a 12-slot -3-dB-coupler in the R140 band. A tandem connection of -8.34-dB sections is utilized, but the whole -3-dB coupling structure has been optimized. The optimum design (Fig. 6(a)) achieves a ± 1-dB bandwidth of the coupling of about 4.4 GHz together with more than 30-dB isolation. The calculated results of Fig. 6(b) (a realized design with somewhat more convenient mechanical dimensions) shows good agreement

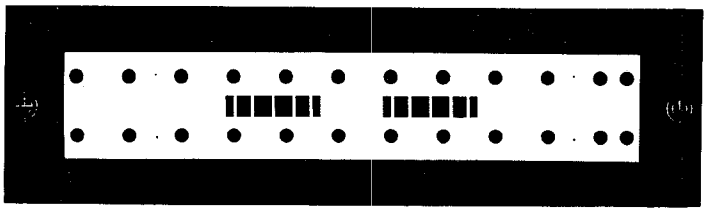

Fig. 7. Photograph of the metal insert containing the metal-etched coupling slots for the *Ku*-band 12-slot coupler of Fig. 6(b). Material: 99.9-percent pure copper, insert thickness $t = 190\ \mu$m. (Two tandem connected -8.34-dB coupling sections, complete -3-dB structure optimized).

between theory and measurements. Fig. 7 shows a photograph of the coupling metal insert containing the 12 metal-etched coupling slots of the fabricated simple R140-band coupler of Fig. 6(b), Table I. The material of the 190-μm-thick insert is 99.9-percent pure copper; the measured deviation from the -3.01-dB coupling insertion loss due to copper losses is less than 0.1 dB.

V. Conclusion

Narrow-wall metal-insert slot couplers achieve coupler designs for the inexpensive and very accurate metal-etching technique advantageously applied recently to waveguide-integrated millimeter-wave filters. A suitable computer-aided design of such filters is based on the method of field expansion in appropriate eigenmodes which allows calculation of the modal scattering matrix and the immediate inclusion of all significant higher order mode coupling effects, also below the corresponding cutoff frequencies. Further, finite wall thickness of the coupling section, and the discontinuity effect at the abrupt change in width of the two waveguides are inherently taken into account by this method. Computer-optimized design data for -20-, -8.34-, and -3-dB couplers are given for the R140 band. The design data are transferable into other frequency bands of interest. The coupling sheet-metal thickness t scaled up to the R180 band ($t \approx 150\ \mu$m), R260 band ($t \approx 100\ \mu$m), and R620 band ($t \approx 50\ \mu$m) are commercially available, like the related value for the R140 band ($t = 190\ \mu$m). Measurements at a two-slot -20-dB and a 12-slot -3-dB coupler prototype show good agreement with theory.

Appendix

Elements of the scattering matrix S^W; change in waveguide width (4):

(Y_i): diagonal matrix with the diagonal elements $1/\sqrt{Z_{FH_i}}$ cf. (2), $i = m, n$

$(1/\beta_i)$: diagonal matrix with the diagonal elements $1/\beta_i$ cf. (2), $i = m, n$

$$(q) = (Y_n)(1/\beta_n)((K_{2mn})(Y_n))^{-1}(Y_m) + (K_{1nm})(Y_m)(1/\beta_m)$$

$$(r) = (Y_n)(1/\beta_n)((K_{2mn})(Y_n))^{-1}(Y_m) - (K_{1nm})(Y_m)(1/\beta_m)$$

$$(s) = (K_{2mn})(Y_n) + (Y_m)((K_{1nm})(Y_m)(1/\beta_m))^{-1} \cdot (Y_n)(1/\beta_n)$$

$$(t) = (K_{2mn})(Y_n) - (Y_m)((K_{1nm})(Y_m)(1/\beta_m))^{-1} \cdot (Y_n)(1/\beta_n) \quad \text{(A1)}$$

with

$$(K_{2mn}) = (K_{1nm})^T, \quad T = \text{transposed}$$

the elements of the coupling matrix (K_{1nm}) are given by

$$K_{1nm} = \frac{2\int_{x_1}^{x_2} \sin\left[\frac{m\pi}{x_2 - x_1}(x - x_1)\right] \sin\left[\frac{n\pi}{x_3}\right] dx}{\sqrt{(x_2 - x_1)x_3}}. \quad \text{(A2)}$$

Elements of the scattering matrix S^B, waveguide bifurcation (6)

$$g = \frac{2}{\sqrt{(a_3 + a_2)(a_2 - a_1)}} \quad h = \frac{2}{\sqrt{(a_3 + a_2)(a_3 - a_1)}} \quad \text{(A3)}$$

(0): zero matrix

(Y_i): cf. (A1)

(Z_i): diagonal matrix with the diagonal elements $\sqrt{Z_{FH_i}}$, $i = m, n, p$

$(1/\beta_i)$: cf. (A1)

(I_{1pn}): coupling matrix with the elements

$$I_{1pn} = \int_{-a_2}^{-a_1} \sin\left[\frac{n\pi}{a_2 - a_1}(x + a_2)\right] \cdot \sin\left[\frac{p\pi}{a_3 + a_2}(x + a_2)\right] dx$$

(I_{2pm}):

$$I_{2pm} = \int_{a_1}^{a_3} \sin\left[\frac{m\pi}{a_3 - a_1}(x - a_1)\right] \cdot \sin\left[\frac{p\pi}{a_3 + a_2}(x + a_2)\right] dx.$$

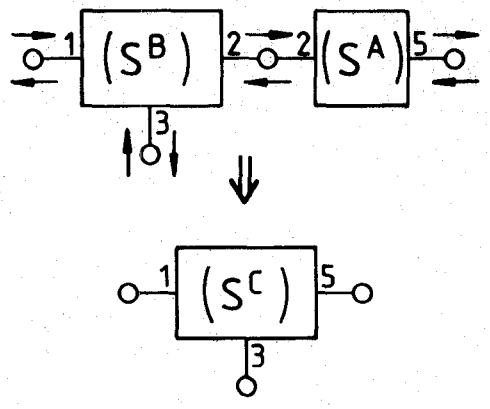

Fig. 8. Scattering matrix (S^C) of a two-port (S^A) cascaded with a three-port (S^B).

Direct combination of a two-port with a three-port scattering matrix (Fig. 8)

$$(S^B) = \begin{pmatrix} (S^B_{11}) & (S^B_{12}) & (S^B_{13}) \\ (S^B_{21}) & (S^B_{22}) & (S^B_{23}) \\ (S^B_{31}) & (S^B_{32}) & (S^B_{33}) \end{pmatrix}$$

$$(S^A) = \begin{pmatrix} (S^A_{22}) & (S^A_{25}) \\ (S^A_{52}) & (S^A_{55}) \end{pmatrix}$$

$$(S^C) = \begin{pmatrix} (S^C_{11}) & (S^C_{15}) & (S^C_{13}) \\ (S^C_{51}) & (S^C_{55}) & (S^C_{53}) \\ (S^C_{31}) & (S^C_{35}) & (S^C_{33}) \end{pmatrix}$$

with

$$(S^C_{11}) = (S^B_{11}) + (S^B_{12})(P_2)(S^B_{21})$$
$$(S^C_{15}) = (S^B_{12})(S^A_{25}) + (S^B_{12})(P_2)(P_4)$$
$$(S^C_{13}) = (S^B_{13}) + (S^B_{12})(P_2)(S^B_{23})$$
$$(S^C_{51}) = (P_3)(S^B_{21})$$
$$(S^C_{55}) = (S^A_{55}) + (P_3)(P_4)$$
$$(S^C_{53}) = (P_3)(S^B_{23})$$
$$(S^C_{31}) = (S^B_{31}) + (S^B_{32})(P_2)(S^B_{21})$$
$$(S^C_{35}) = (S^B_{32})(S^A_{25}) + (S^B_{32})(P_2)(P_4)$$
$$(S^C_{33}) = (S^B_{33}) + (S^B_{32})(P_2)(S^B_{23})$$

where

$$(P_1) = (U) - (S^B_{22})(S^A_{22})$$
$$(P_2) = (S^A_{22})(P_1)^{-1}$$
$$(P_3) = (S^A_{52})(P_1)^{-1}$$
$$(P_4) = (S^B_{22})(S^A_{25})$$
(U): unity matrix.

Acknowledgment

The authors thank D. Grauerholz for checking the design data, constructing the prototype couplers, and for the measurements.

References

[1] N. Marcuvitz, *Waveguide Handbook*. New York: McGraw-Hill, 1951, pp. 378–379.
[2] R. Levy, "Directional couplers," in *Advances in Microwaves*, L. Young, Ed. London: Academic Press, 1966, vol. 1, pp. 137–139, 151–154.
[3] H. J. Riblet, "The short slot hybrid junction," *Proc. IRE*, vol. 40, pp. 180–184, Feb. 1952.
[4] W. Stoesser, "Der 3-dB-koppler," *Frequenz*, vol. 14, pp. 117–121, Apr. 1960.
[5] H. Kaden, "Elektromagnetische Wellen in Verzweigungen von Rechteckhohlleitern," *Arch. Elek. Übertragung.*, vol. 15, pp. 61–70, Feb. 1961.
[6] I. Lucas, "Allgemeine Theorie des Kurzschlitz–Richtungskopplers," *Arch Elek. Übertragung.*, vol. 21, pp. 339–344, 1967.
[7] K. Tomiyasu and S. B. Cohn, "The Transvar directional coupler," *Proc. IRE*, vol. 41, pp. 922–926, July 1953.
[8] S. E. Miller, "Coupled wave theory and waveguide applications," *Bell Syst. Tech. J.*, vol. 33, pp. 661–719, 1954.
[9] S. E. Miller and W. W. Mumford, "Multielement directional couplers," *Proc. IRE*, vol. 40, pp. 1071–1078, 1952.
[10] R. Vahldieck, J. Bornemann, F. Arndt, and D. Grauerholz, "Optimized waveguide *E*-plane metal-insert filters for millimeter-wave applications," *IEEE Trans. Microwave Theory Tech.*, vol. MTT-31, pp. 65–69, Jan. 1983.
[11] F. Arndt, B. Koch, H.-J. Orlok, and N. Schröder, "Field theory design of rectangular waveguide broad-wall metal-insert slot couplers for millimeter-wave applications," *IEEE Trans. Microwave Theory Tech.*, vol. MTT-33, pp. 95–104, Feb. 1985.
[12] H. Patzelt and F. Arndt, "Double-plane steps in rectangular waveguides and their application for transformers, irises, and filters," *IEEE Trans. Microwave Theory Tech.*, vol. MTT-30, pp. 771–776, May 1982.
[13] T. Tanaka, "Ridge-shaped narrow wall directional coupler using TE_{10}, TE_{20}, and TE_{30} modes," *IEEE Trans. Microwave Theory Tech.*, vol. MTT-28, pp. 239–245, Mar. 1980.
[14] R. E. Collin, *Field Theory of Guided Waves*. New York: McGraw-Hill, 1960, pp. 338–359, 447–449, 22–27.
[15] H. Schmiedel, "Feldtheoretische Analyse und Synthese von Modenkopplern," *Frequenz*, vol. 39, pp. 207–214, Aug. 1983.
[16] T. E. Rozzi and W. F. G. Mecklenbräuker, "Wide-band network modeling of interacting inductive irises and steps," *IEEE Microwave Theory Tech.*, vol. MTT-23, pp. 235–245, Feb. 1975.
[17] M. S. Navarro, T. E. Rozzi, and Y. T. Lo, "Propagation in a rectangular waveguide periodically loaded with resonant irises," *IEEE Trans. Microwave Theory Tech.*, vol. MTT-28, pp. 857–865, Aug. 1980.
[18] H. Schmiedel, "Anwendung der Evolutionsoptimierung bei Mikrowellenschaltungen," *Frequenz*, vol. 35, pp. 306–310, Nov. 1981.

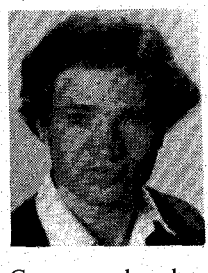

Heinz Schmiedel was born in Odenhausen/Lahn, Germany, on May 7, 1953. He received the Dipl.-Ing. and Dr.-Ing. degrees in electrical engineering from the University of Bremen, Bremen, Germany, in 1979 and 1983, respectively. There he was involved in the design of stripline couplers, waveguide components, and optimization techniques.

In 1983, he joined the Deutsche Bundespost. Since 1985, he has been with the Research Institute of the Deutsche Bundespost, Darmstadt, Germany, where he works on wave propagation.

Fritz Arndt (SM'83) was born in Konstanz, Germany, on April 30, 1938. He received the Dipl.-Ing., the Dr.-Ing., and the Habilitation degrees from the Technical University of Darmstadt, Germany, in 1963, 1968, and 1972, respectively.

From 1963 to 1972, he worked on directional couplers and microstrip techniques at the Technical University of Darmstadt. Since 1972, he has been a Professor and Head of the Microwave Department at the University of Bremen, Germany. His research activities are, at present, in the area of the solution of field problems of waveguide, finline and optical waveguide structures, antenna design, and scattering structures.

Dr. Arndt is member of the VDE and NTG (Germany). In 1970, he received the NTG Award, and in 1982 the A. F. Bulgin Award (together with three coauthors) from the Institution of Radio and Electronic Engineers.